Bioactivity of Biosilica Obtained From North Atlantic Deep-Sea Sponges

Olesia Dudik[1,2], Sara Amorim[1,2], Joana R. Xavier[3,4], Hans Tore Rapp[4], Tiago H. Silva[1,2]*, Ricardo A. Pires[1,2]* and Rui L. Reis[1,2]

[1] 3B's Research Group, I3Bs – Research Institute on Biomaterials, Biodegradables and Biomimetics, University of Minho, Headquarters of the European Institute of Excellence on Tissue Engineering and Regenerative Medicine, Guimarães, Portugal, [2] ICVS/3B's - PT Government Associate Laboratory, Guimarães, Portugal, [3] CIIMAR – Interdisciplinary Centre of Marine and Environmental Research, Terminal de Cruzeiros de Leixões, Matosinhos, Portugal, [4] Department of Biology and K.G. Jebsen Centre for Deep-sea Research, University of Bergen, Bergen, Norway

Demosponges are a well-known source of a plethora of bioactive compounds. In particular, they are able to form a skeleton by direct deposition of silica in a process catalyzed by silicatein. Herein, we isolated biosilicas from five different Atlantic deep-sea sponges *Geodia atlantica* (GA), *Geodia barretti* (GB), *Stelletta normani* (SN), *Axinella infundibuliformis* (AI), and *Phakellia ventilabrum* (PV) to explore the bioactivity and osteogenic capacity of its silica-based materials. We chemically characterized the isolated biosilicas and evaluated them for their bioactivity to deposit Ca and P on their surface (by immersion in simulated body fluid, SBF). GB-, SN-, AI-, and PV-based biosilicas did not generate a stable calcium phosphate (CaP) layer over time in the presence of SBF, however, the GA-derived one was able to form a CaP surface layer (at a Ca/P ratio of ∼1.7, similar to the one observed for hydroxyapatite), that was stable during the 28 days of testing. In addition, no cytotoxicity toward L929 and SaOs2 cells was observed for the GA-based biosilica up to a concentration of 10 mg/mL. Overall, the GA-based biosilica presents the characteristics to be used in the development of biomaterials for bone tissue engineering (BTE).

Keywords: bioactivity, biosilica, bioceramics, tissue engineering, deep-sea sponges

INTRODUCTION

The marine environment is a source of a wide range of compounds, which have been subject of intense research due to their potential biomedical application. It has been reported the extracted and purified marine-origin chemicals present antibiotic, anticancer, anti-inflammatory and antiviral activities, among many others (Marris, 2006). In addition, silica-based chemical structures, as the ones found in marine sponges (Thakur and Müller, 2004; Venkatesan et al., 2016), have the potential to be used as bioactive and osteogenic biomaterials relevant for bone tissue engineering (BTE) applications.

The most common way used by marine sponges to produce their biosilica-based skeleton is through deposition/assembly catalyzed by silicatein (i.e., α, β, and γ isoforms). During this process, siliceous spicules are formed through the direct deposition of silica along the axial direction of the silicatein filaments (Cha et al., 1999; Müller et al., 2008; Ehrlich et al., 2010a).

Biosilica represents the main component of the matrix of these spicules (Ehrlich et al., 2010b; Kulakovskaya et al., 2012; Wang et al., 2012); however, collagen, being the predominant protein in the organic matrix of marine sponges, is also present. In this sense, sponge spicules are regarded as a composite material (Schröder et al., 2008). In addition, several reports demonstrated that biogenic polyphosphates (linear inorganic polymers) are also involved in the formation of biosilica (Kulaev et al., 2005).

The hierarchical organization of sponge skeletons and spicules containing amorphous silica (classes Demospongiae, Hexactinellida, and Homoscleromorpha) or calcium carbonate (class Calcarea) inspired researchers to use them in the development of biomaterials for BTE (Silva et al., 2012; Barros et al., 2014; Odatsu et al., 2015; Lewandowska-Łańcucka et al., 2015; Antoniac et al., 2016; Wysokowski et al., 2018). The use of this biosilica has been considered as a promising biomimetic approach to recapitulate the inorganic part of the bone extracellular matrix (ECM) (Dudik et al., 2018).

It has been shown that biosilica promotes osteoblast proliferation and function (Wang et al., 2013). In fact, Schröder et al. reported that the silica-containing bioactive surfaces generated through silicatein-mediated catalysis induce the formation of hydroxyapatite (HA) crystals under SaOs2 cell culture (Schröder et al., 2005). Wiens et al. (2010a,b) also revealed the osteogenic potential of biosilica in their studies, showing that it is able to promote the formation of HA crystals and increase the gene expression of SaOs2 cells. More recently, Barros et al. demonstrated that ceramic structures obtained upon calcination of marine sponges (i.e., *Petrosia ficiformis*, *Agelas oroides*, and *Chondrosia reniformis*) are non-cytotoxic and have the potential to be used as substitutes of synthetic Bioglass (Barros et al., 2016).

A wide range of bioceramic-based strategies, typically using calcium phosphates (CaP) and/or bioactive glasses, or polymers (e.g., naturally derived collagen type I), as well as hybrid materials, created by the mixture of bioceramics and polymeric structures, have been developed targeting BTE (Rezwan et al., 2006; Fu et al., 2011; Amorim et al., 2014; Fernandes et al., 2016). In the case of bioactive silica-based glasses, they are able to bind and integrate into the bone tissue through the formation of a silica gel layer. It is reported that this layer attracts and stimulates osteoprogenitor cells to proliferate and to differentiate into osteoblasts, which, in turn, start the synthesis and deposition of ECM and its mineralization (Blunt et al., 2005; Blunt et al., 2010). Fabrication of glass and glass-ceramic scaffolds with architectures mimicking the 3D interconnected porosity of natural bone has been explored (Rezwan et al., 2006; Rahaman et al., 2011; Kaur et al., 2014). In general, adequate mechanical strength and controlled degradation rates are two of the most relevant properties for application to a BTE strategy.

Within the use of composites as biomaterials for BTE, marine building blocks are establishing a representative role (Silva et al., 2012), namely following the studies reporting the use of: collagen combined with calcium phosphates (Elango et al., 2016; Diogo et al., 2018, 2020); biosilica from sponges (Müller et al., 2004), but also from diatoms (Le et al., 2018); polyphosphates inspired in the materials found in sponges (Wang et al., 2018);

among many others. Interest in marine biomaterials for BTS has been associated with the sustainable production methodologies, namely benefiting from strategies proposed for the valorization of marine by-products, such as fish bones and skins, but also due to the absence of ethical or health constraints, which are usually associated with the use of mammal-derived components.

Herein, we focus on the evaluation of the biomedical potential of biosilica derived from five North Atlantic deep-sea sponge species of the class Demospongiae, namely *Geodia atlantica* (GA), *Geodia barretti* (GB), *Stelletta normani* (SN) (order Tetractinellida), and *Axinella infundibuliformis* (AI), *Phakellia ventilabrum* (PV) (order Axinellida). We report on their physicochemical characterization, bioactivity (herein referred as the ability to promote the formation of CaP layer on the surface of the biosilicas) and cytotoxicity under *in vitro* conditions, as a screening methodology to develop marine-based biosilica structures with potential to be used in BTE.

MATERIALS AND METHODS

Materials
Sponge Samples
Sponge samples of the species *Geodia atlantica* (GA), *Geodia barretti* (GB), *Stelletta normani* (SN), *Axinella infundibuliformis* (AI), and *Phakellia ventilabrum* (PV) were collected in Korsfjord, Norway, using a triangular dredge, at depths between 332 and 97 m for GA, GB, PV and between 292 and 226 m for SN and AI. Upon collection, samples were fragmented and preserved in 99% ethanol. Taxonomic identifications were made from the analyses of external and internal morphological characteristics. Representative fragments, i.e., comprising both the sponge ectosome (external part) and choanosome (inner part), were selected for further materials processing and characterization.

Chemicals
Sodium chloride (PanReac AppliChem, Spain), sodium hydrogen carbonate (Merck, Germany), potassium chloride (VWR International, Portugal), di-potassium hydrogen phosphate trihydrate (Merck, United Kingdom), Tris(hydroxymethyl)-aminomethane, magnesium chloride hexahydrate and calcium chloride (Sigma-Aldrich, Portugal), sodium sulfate (Sigma-Aldrich, Australia), hydrochloric acid (Fisher Scientific, United Kingdom) were used for preparation of simulated body fluid (SBF). All the reagents were ACS reagent grade. 1,000 mg/L Ca ICP standard solution (Alfa Aesar, Germany) and 1,000 mg/L P ICP standard solution (Merck, Germany) were used for preparation of calibration standards. Ultrapure water was used throughout the study.

Extraction of Bioceramics From Deep-Sea Sponges
The marine sponges were calcinated in a furnace (FornoCeramica, Portugal) at 800°C for 6 h in order to remove the whole organic components thereby extracting the inorganic part. Prior to the calcination process, the samples were cut into pieces and washed repeatedly with ultrapure water.
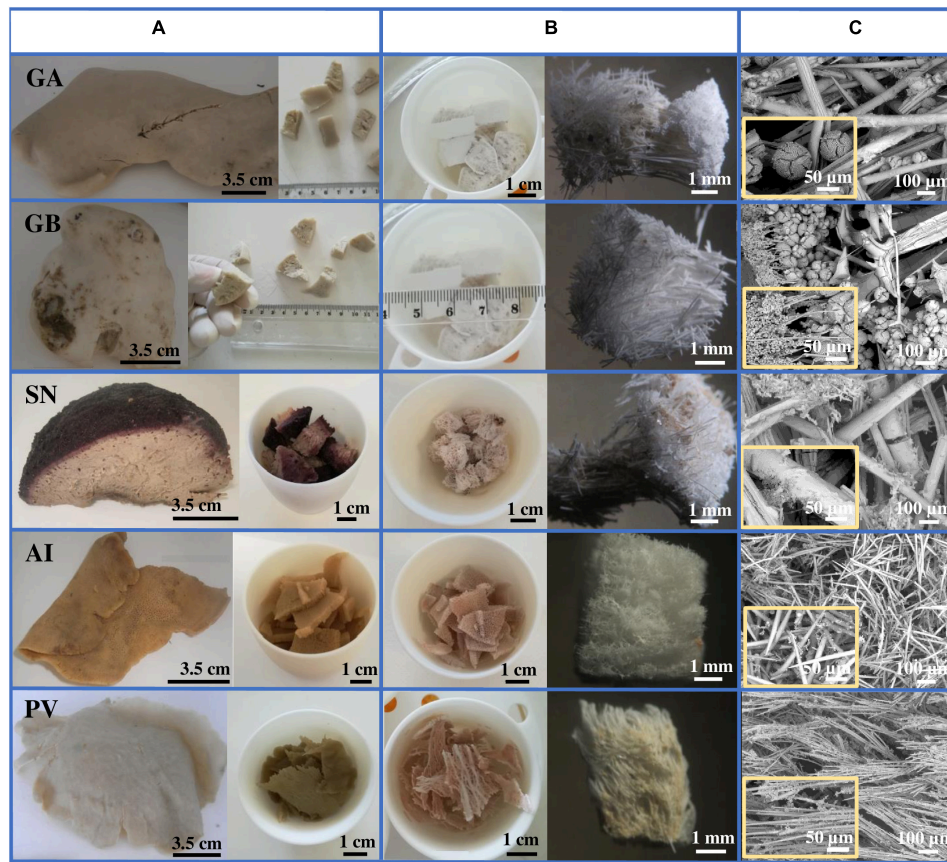
FIGURE 1 | (A) GA, GB, SN, AI, and PV marine sponge specimens and corresponding sponge pieces before calcination. **(B)** Corresponding sponge-derived biosilicas obtained upon calcination and close-up of each calcined sponge piece. **(C)** SEM images showing silica-based spicules obtained upon calcination.

TABLE 1 | Quantification of the chemical elements present in the biosilicas obtained from the different marine sponges.

Sponge species	Composition (Wt%)								
	O	Si	Ca	Na	P	Mg	K	S	Al
GA—*Geodia atlantica*	54.0	37.5	1.9	2.5	1.6	0.9	1.3	0.4	–
GB—*Geodia barretti*	53.3	38.4	1.2	3.2	0.7	0.8	0.8	0.2	1.3
SN—*Stelletta normani*	53.7	36.6	2.7	1.9	1.1	1.0	0.8	0.8	1.4
AI—*Axinella infundibuliformis*	54.8	35.1	2.7	2.0	1.5	1.7	0.8	1.1	0.3
PV—*Phakellia ventilabrum*	53.3	39.2	1.9	1.2	0.7	0.7	0.9	0.6	1.5

Bioactivity Assessment

The biosilicas obtained from the different marine sponges were immersed in SBF. The SBF was prepared according to the procedure described by Kokubo and Takadama (2006). The initial concentrations of calcium and phosphorus ions in SBF were 2.5 and 1 mmol/L, respectively. The samples were immersed in SBF using plastic tubes, under a powder-to-liquid ratio of 1.5 mg:
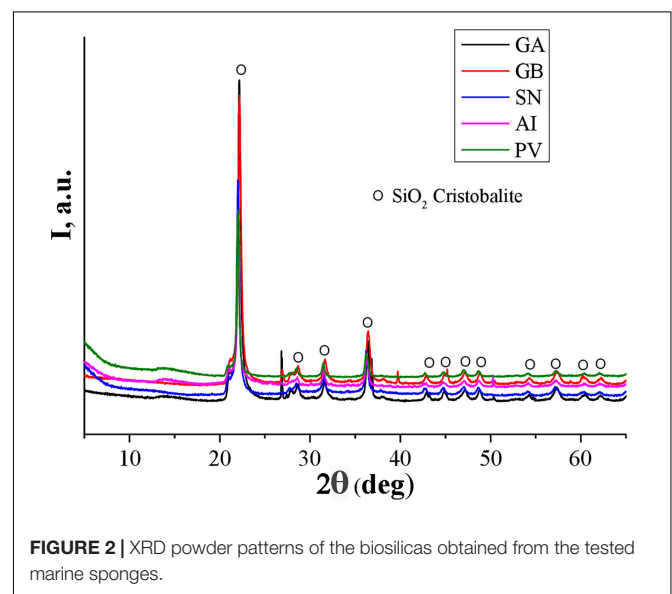

FIGURE 2 | XRD powder patterns of the biosilicas obtained from the tested marine sponges.

1 mL (Jones et al., 2001; Yu et al., 2012; Greasley et al., 2016), using aliquots of 15 mg of each biosilica per 10 mL of SBF. Samples were placed in a thermostatic water bath at 37°C, for 6 h,
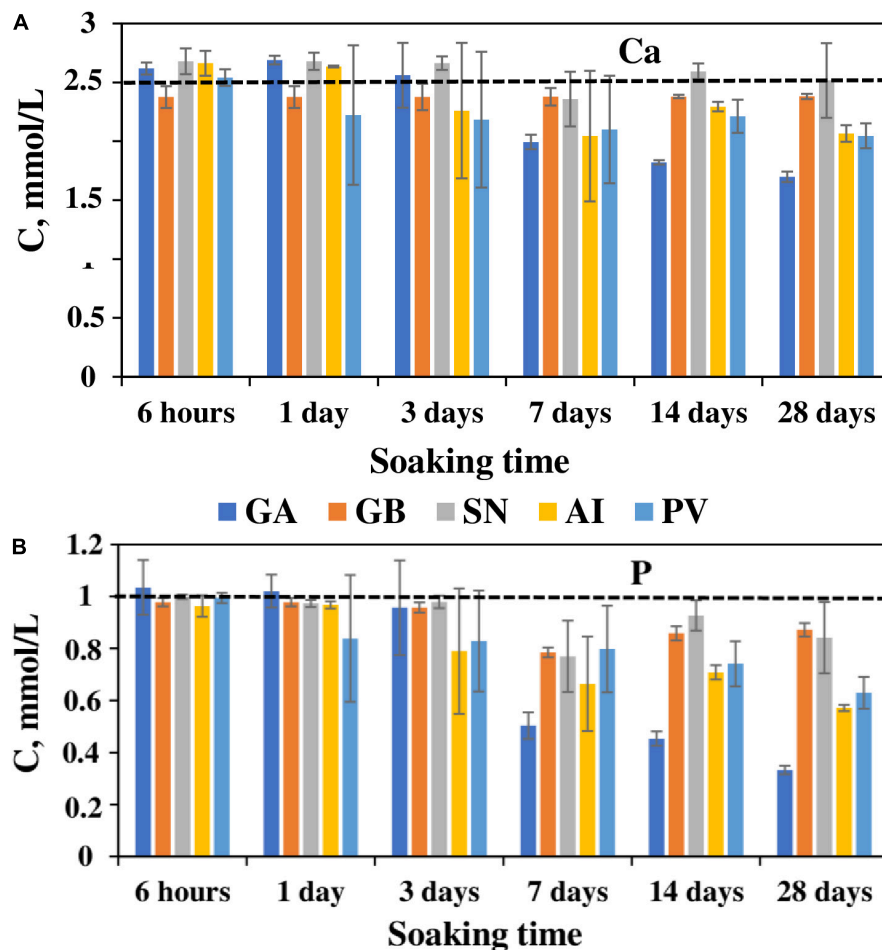
FIGURE 3 | Changes in Ca **(A)** and P **(B)** concentrations in the SBF solutions after immersion of the different biosilicas during 28 days.

1, 3, 7, 14, and 28 days under constant agitation (i.e., 60 rpm). Three samples of each biosilica were used per test, with average values reported. At each time point the SBF was separated from the solid and used to determine the Ca and P concentrations. The solid was washed with distilled water, dried at 37°C and assessed microscopically.

Characterization of the Biosilica Surface
Scanning Electron Microscopy and Energy Dispersive X-Ray Spectroscopy
Scanning electron microscopy (SEM) was carried out on a JSM-6010 LV microscope (JEOL, Japan) equipped with an energy dispersive (EDS) x-ray spectroscope (Oxford Instruments, United Kingdom) under a working distance of 10–12 mm and a beam energy of 10.0 kV. The low vacuum mode allowed non-conductive biosilicas (samples before grinding) to be observed and analyzed without conductive coating. Powders of biosilicas before and after immersion in SBF were platinum coated (apx. 2 nm) prior to the analysis. EDS analysis was performed at four points using a beam energy of 15.0 kV and a magnification of 500×. EDS spectra were analyzed using the

Aztec software from Oxford Instruments) and presented as a semi-quantitative evaluation.
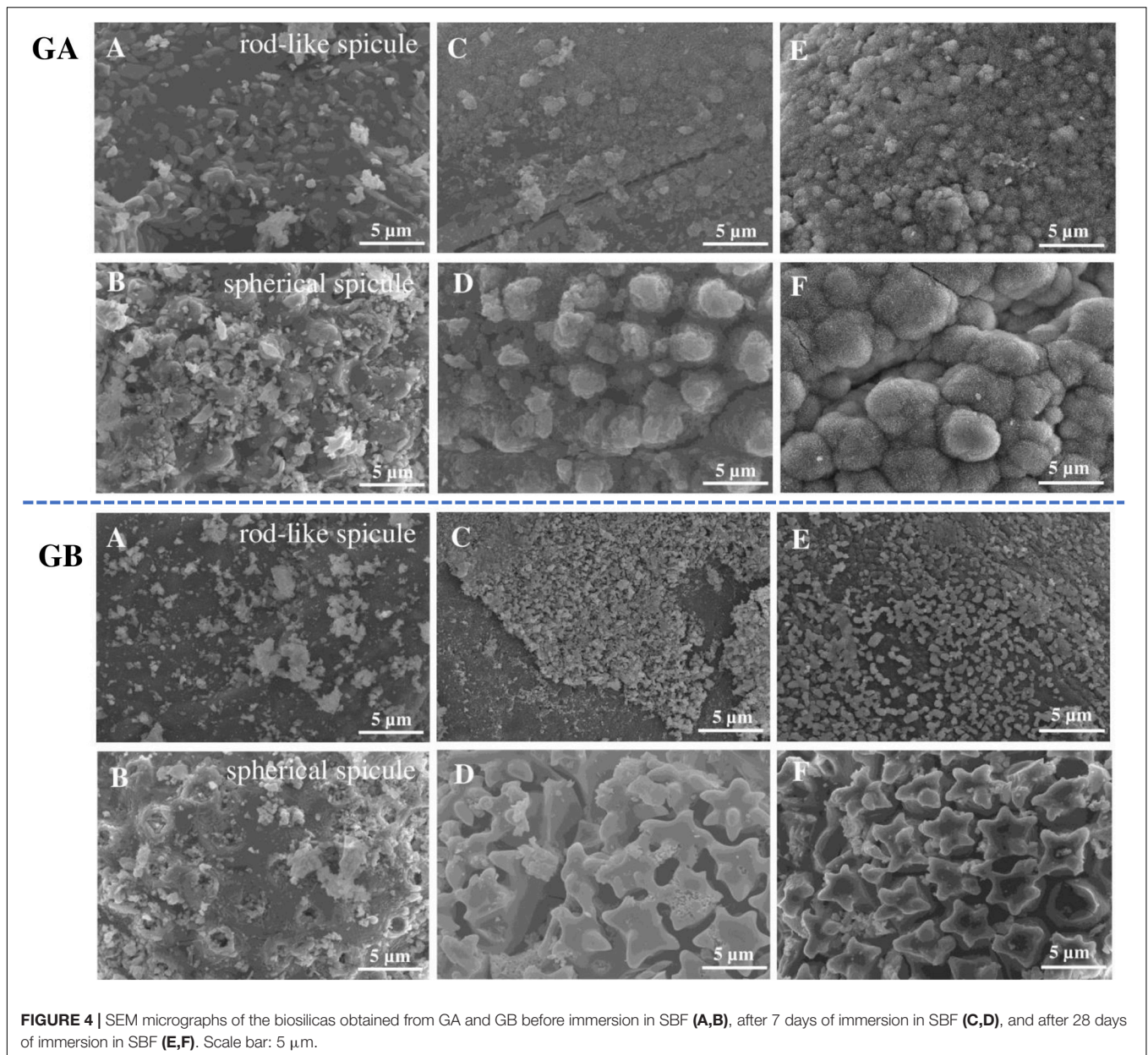
Fourier Transform Infrared Spectroscopy
Fourier transform infrared spectroscopy (FTIR) spectra were collected on an IR Prestige-21 spectrometer (Shimadzu, Japan) as an average of 32 scans, a wavenumber range between 4,000 and 400 cm^{-1} and a resolution of 4 cm^{-1}. A press (Pike, United States) was used to prepare transparent pellets containing biosilica powders mixed with potassium bromide.

X-Ray Diffraction
X-ray diffraction (XRD) analysis was executed on a XRD diffractometer (Bruker D8 Advance, Germany), operating using a Cu-Kα radiation in θ/2θ mode, in the range between 6° and 70°, using a step increment of 0.04° and an acquisition time of 1 s per step.

Thermogravimetric Analysis
Thermogravimetric analysis of the sponge samples was carried out on Simultaneous Thermogravimetric Analyzer STA7000 (Hitachi, Japan) under a temperature range from 23 to 800°C

FIGURE 4 | SEM micrographs of the biosilicas obtained from GA and GB before immersion in SBF **(A,B)**, after 7 days of immersion in SBF **(C,D)**, and after 28 days of immersion in SBF **(E,F)**. Scale bar: 5 µm.

and a heating rate of 10°/min in an oxygen atmosphere. For each biosilica, it was used a sample weight of 8–10 mg.

Inductively Coupled Plasma Optical Emission Spectrometry

Inductively coupled plasma—optical emission spectrometry (ICP-OES) was used to determine the Ca and P concentrations present in the SBF before and after the immersion of the biosilicas. The ICP-OES analysis was performed on a ICP spectrometer (HORIBA JY 2000-2, United States), using the absorption wavelengths of $\lambda = 317.93$ nm and $\lambda = 214.91$ nm for Ca and P, respectively. Concentrations of Ca and P were calculated from standard calibration curves prepared using standard solutions from 0 to 10 ppm.

Cytotoxicity Studies

The cytotoxicity of the biosilicas was evaluated following an established protocol based on ISO/EN 10 993 standard (ISO 10993-5, 2009) guidelines, using an immortalized mouse lung fibroblast cell line (L929) and Sarcoma cell line (SaOs2) purchased from the European Collection of Cell Cultures. In brief, biosilicas (100, 50, and 10 mg/mL; 3 samples from the biosilica obtained from the same sponge were used throughout the analysis) were incubated in DMEM culture medium (Dulbecco's Modified Eagle's Medium—low glucose) with 10% heat-inactivated fetal bovine serum (FBS; Biochrom AG, Germany) and 1% antibiotic/antimycotic solution (containing a final concentration of penicillin 100 units/mL and streptomycin 100 mg/mL; Gibco, United Kingdom), for

TABLE 2 | Chemical composition of the surface of the biosilicas after 28 days of immersion in simulated body fluid (SBF).

Sponge species	Composition (Wt%)								
	O	Si	Ca	Na	P	Mg	K	S	Al
GA—*Geodia atlantica*	54.3	15.4	18.6	0.4	10.6	0.7	–	–	–
GB—*Geodia barretti*	55.0	37.9	2.2	1.1	1.9	0.5	0.3	–	0.9
SN—*Stelletta normani*	56.6	39.4	0.7	0.7	0.3	0.5	0.4	–	1.4
AI—*Axinella infundibuliformis*	54.8	40.3	1.2	0.8	0.9	1.2	0.5	–	0.2
PV—*Phakellia ventilabrum*	56.0	42.0	0.8	0.3	0.4	0.2	0.3	–	–

24 h in a water bath at 37°C and 60 rpm. The leachables of each sample were collected and filtered using a 0.22 μm syringe filter. L929 and SaOs2 cells (11,000 cells.cm^{-2}) were cultured in a 96-well plate in DMEM and after 24 h, the media were replaced by the collected biosilica extracts. Cell viability was evaluated by AlamarBlue assay after 24 and 72 h. The percentage of reduced AlamarBlue was calculated according to the manufacturer instructions (Bio-Rad). The results presented were normalized to the absorbance obtained for control cells cultured in DMEM (positive control) and correspond to the average of three measurements (±standard deviation).

Statistical Analysis

The data obtained from the ICP analysis and cytotoxicity tests were expressed as mean ± standard deviation (SD). The statistical analysis of the cytotoxicity study was performed by using the Shapiro-Wilk test ($p < 0.05$) to check if the data presented a normal distribution. The data did not follow a normal distribution and, as a consequence, were analyzed using the Mann-Whitney test. The statistically significant differences are represented with * for $p < 0.05$ and ** for $p < 0.01$.

RESULTS AND DISCUSSION

Characterization of the Biosilica Samples

Biosilica structures were obtained after calcination of the sponges (**Figures 1A,B**, before and after treatment) as described in the methods section. In all the cases, the biosilicas were fragile 3D structures composed of siliceous spicules with different sizes and shapes (**Figure 1B**). The elimination of the organic matrix resulted in an amount of loose spicules, indicating that the spicules were embedded into the organic matrix which, upon calcination, lost its solid support. Moreover, SEM analysis confirmed that all the spicules were cracked after the calcination step, probably due to the degradation of the organic components, such as proteins (e.g., silicateins and collagen) that occurs during the heating process (**Figure 1C**). The microscopic observation of the biosilicas obtained from GA and GB revealed the presence of different types of spicules, such as sterrasters (microscleres, spherical) and dichotriaenes (megascleres), which have been previously reported and reviewed (Cárdenas et al., 2013).

Thermogravimetric analysis showed that the organic portion of the marine sponges were removed upon calcination at 800°C during 6 h, with the silica content of these sponges accounting to about 50–60% of their dry mass (**Supplementary Figure 1**, example of TG and DTG curves obtained for GB). The weight loss observed in the lower temperature region (i.e., $T_{max} \sim 100°C$, weight loss $\sim 8\%$) is attributed to water desorption. Further weight loss in the temperature region between 200 and 544°C with a total mass loss of about 40% corresponds to the thermal decomposition of the sponge's organic components.

EDS, XRD, and FTIR analysis showed that the inorganic part of the marine sponges is mainly composed of silicates, compatible with biosilica spicules. However, EDS data revealed that they also contained traces of other elements, such as Ca, Na, P, Mg, K, and S. Moreover, Al was also found, but only in the biosilicas obtained from GB, SN, AI, and PV (**Table 1**). The elemental composition of the biosilicas demonstrates their inherent ability to bind to other essential cations, such as Ca^{2+}, Mg^{2+}, K^+, Na^+, and Al^{3+}. In their FTIR spectra (**Supplementary Figure 2**), the shoulder at apx. 1,650 cm^{-1} can be attributed to adsorbed water. The bands at 1,099 and 790 cm^{-1} are assigned to the O-Si-O asymmetrical and symmetrical stretching vibrations, respectively, from the Si-O-Si network. The broad band at $\sim$3,425 cm^{-1} corresponds to the stretching vibrations of −OH from the Si-OH moieties (Khan et al., 2017).

The XRD powder patterns (**Figure 2**) of the biosilicas obtained upon calcination revealed the presence of the most intense peak at 22° 2θ and less intense peaks between 28 and 65° 2θ, which correspond to Cristobalite crystalline phase (COD 9015087) (Xue et al., 2015), confirming that the main structural inorganic component of the sponges are silicates.

Assessment of Bioactivity

To assess the bioactivity of the generated biosilicas (herein referred as the ability of the biosilicas to promote the deposition of CaP layer on their surface), samples were immersed in SBF for different timeframes. At each timepoint, the solution was filtered and analyzed by ICP to determine the Ca and P concentrations. After separation of the biosilica materials from the SBF solution, their surface morphology was analyzed by SEM, while EDS was used to quantify the Ca and P concentrations present in the inorganic structures formed on the surface of the biosilicas.

ICP analysis of the SBF solutions, at the different timepoints of the evaluation of the bioactivity (**Figure 3**), demonstrated that the concentration of Ca and P in the SBF solution increased for several samples up to day 1 (increase of Ca concentration for the biosilicas generated from GA, SN, AI, and increase of P concentration for GA-based biosilica). This could be explained by the diffusion of Ca and P ions present in the biosilica samples into the SBF. Afterwards, for the GB-, SN-, AI-, and PV-derived biosilicas, a decrease of Ca and P concentration was observed between day 1 and day 7, followed by a stabilization up to day 28, showing that these ions were responsible for the formation of a CaP layer on their surfaces. The GA-based biosilicas had an overall higher consumption of Ca and P from SBF leading to its
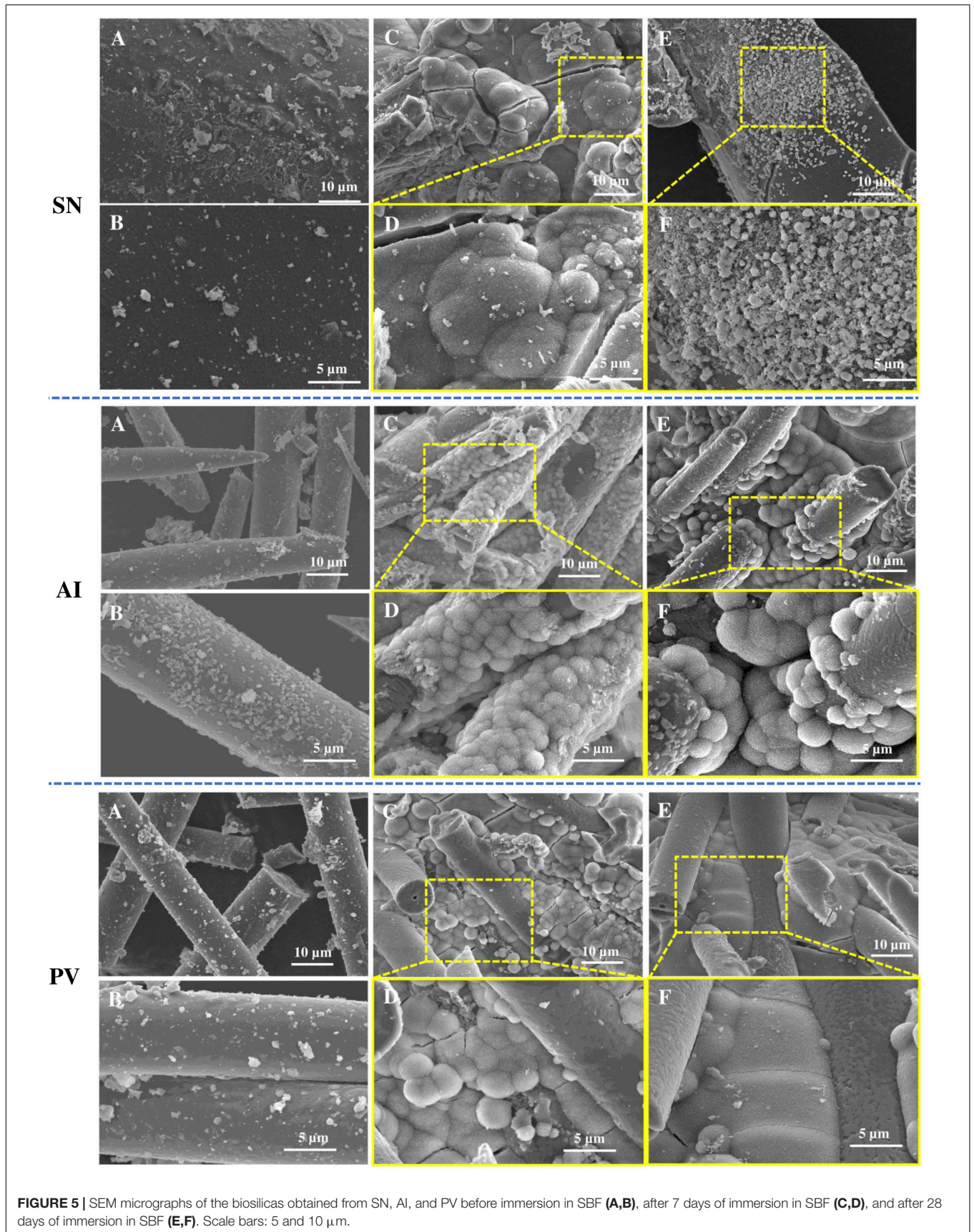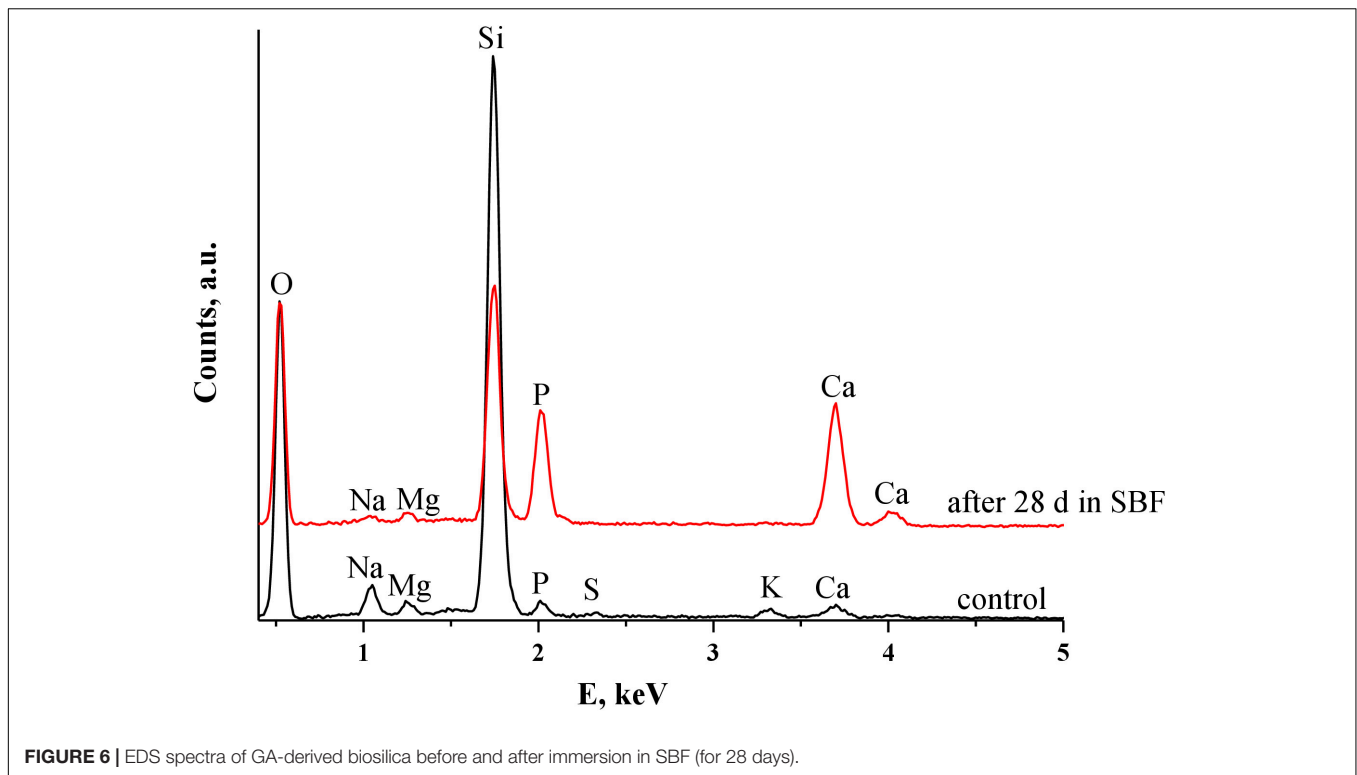
FIGURE 5 | SEM micrographs of the biosilicas obtained from SN, AI, and PV before immersion in SBF **(A,B)**, after 7 days of immersion in SBF **(C,D)**, and after 28 days of immersion in SBF **(E,F)**. Scale bars: 5 and 10 μm.

FIGURE 6 | EDS spectra of GA-derived biosilica before and after immersion in SBF (for 28 days).

deposition on the biosilica surface between day 3 and day 28 (as shown in the SEM analysis, **Figure 4**).

The formation of the CaP layer on the biosilica surface was monitored by SEM and EDS. SEM observation showed that, after immersion in SBF for 28 days, GA-based biosilicas presented the formation of cauliflower structures typical of hydroxyapatite (HA) on the surface of both types of spicules (**Figure 4**). Moreover, the EDS analysis (**Table 2**) showed that the detected CaP structures present a Ca/P ratio of ∼1.7, which is similar to the one expected to be present in HA, confirming its presence in the biosilica surface (Bailey et al., 2009). In contrast to these results, GB-based biosilicas, after immersion in SBF for 7 days, presented dispersed CaP structures only on the rod-like spicules, that noticeably decrease through the 28 days of the evaluation of bioactivity (**Figure 4**).

In the case of the spicules obtained from the SN, PV-, and AI-based biosilicas the formation of dispersed CaP deposits was observed on their surface throughout the whole 28 days of testing. However, especially in the case of the SN-derived biosilica, an additional reduction of CaP deposits was detected after 28 days of immersion (**Figure 5**), confirming that the generated CaP structures are not stable over longer timeframes.

In general, the SEM/EDS data are consistent with the results obtained by ICP, revealing a significant and stable increase in Ca and P content only on the surface of GA-based biosilica after immersion in SBF for 28 days (**Figure 6** and **Table 2**). In fact, it has been previously reported that the bioactivity of biosilicas is correlated with their chemical composition (Barros et al., 2016), where the presence of Ca, Mg, and P promotes the nucleation and growth of HA on their surface, while biosilicas that do not

contain Ca, Mg, nor P, did not show any inherent bioactivity. We did not confirm this trend in the biosilicas obtained from the species herein studied, as all of them presented similar values of Ca/Mg/P concentrations, however, it is relevant to point out that the GA-based biosilica (the one with higher bioactivity) is, in fact, the one that had the higher concentration of P in its initial composition (**Table 1**). Our results give a strong evidence that the GA-based biosilica should be able to promote the regeneration of bone tissue and, consequently, it is highly relevant for the development of BTE strategies. However, this evaluation was executed using chemical methodologies that do not guarantee *per si* the cytocompatibility of the tested biosilica formulations.

Evaluation of Cytotoxicity

To guarantee that the proposed formulations can indeed be used under the biological environment, we tested the cytotoxicity of the developed sponge-based biosilicas. L929 and SaOS2 cells were cultured in the presence of extracts from the biosilicas generated from the sponges GA, GB, SN, AI, and PV. In the cases of GB, SN, AI, and PV, a cellular metabolic activity was detected between 65 and 100%, demonstrating the non-cytotoxic behavior of the biosilica originating from these sponges (**Figure 7**). The GA-based biosilica was non-cytotoxic only at a concentration of 10 mg/mL, being toxic for the highest concentrations, i.e., 50 and 100 mg/mL. The non-cytotoxic behavior of the herein tested biosilicas (which is concentration dependent in the case of GA) suggest their potential use in the BTE. Of note, the metabolic activity of the SaOs2, when in contact with GB− (10 mg/mL) and SN-based (100 mg/mL) biosilicas after 72 h, is higher than the control experiment.
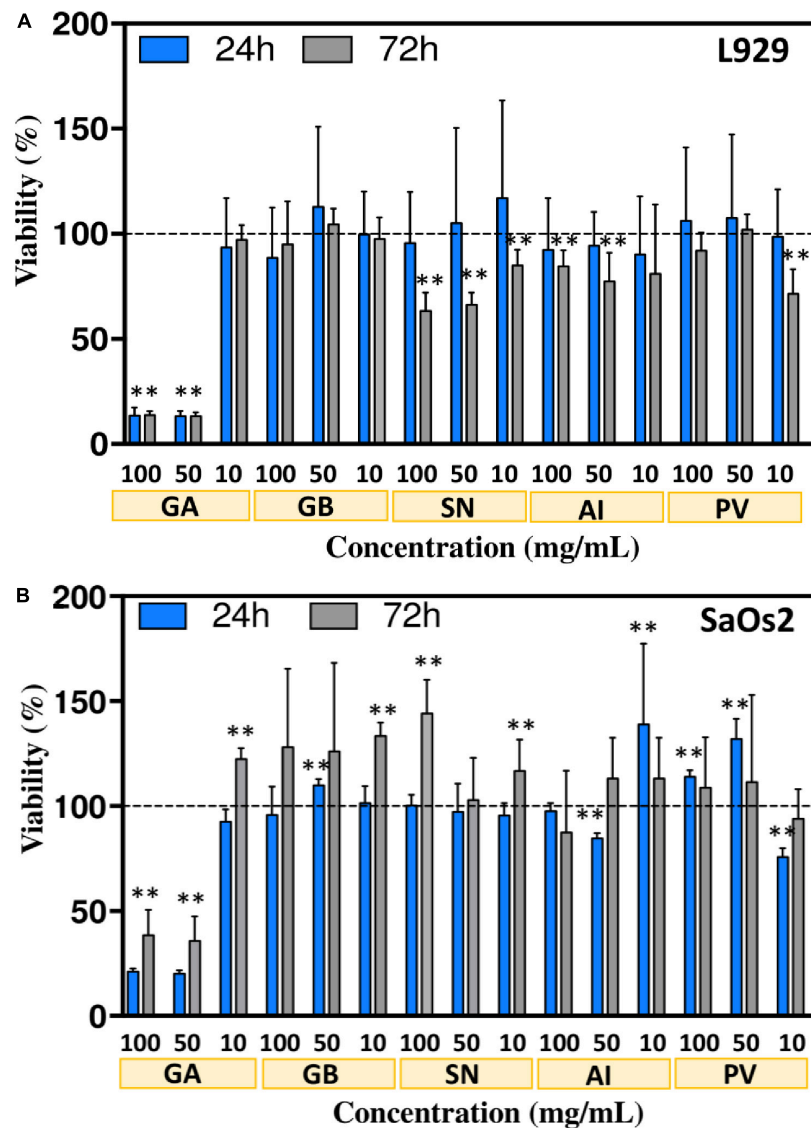
FIGURE 7 | Viability of L929 **(A)** and SaOs2 **(B)** cells, measured using the AlamarBlue assay, when cultured in contact with different concentrations of the extracts from the sponge-based biosilicas, i.e., 10, 50, and 100 mg/mL. Metabolic activity was evaluated after 24 and 72 h of cell culture. The data are presented as mean ± SD and the statistical differences are represented with * for $p < 0.05$ and ** for $p < 0.01$.

Barros et al. (2016) previously evaluated the suitability of different biosilicas as substitutes of synthetic Bioglass, by assessing the metabolic activity of L929 cells in the presence of extracts from biosilicas of the species *Petrosia ficiformis*, *Agelas oroides*, and *Chondrosia reniformis*. In all the cases the cell metabolic activity was between 80 and 100% confirming their non-cytotoxic character. In addition, Gabbai-Armelin et al. (2019) showed that extracts from biosilica obtained from *Tedania ignis* and *Dragmacidon reticulatum* marine sponges, at a concentration of 50 mg/mL, promoted the increment of cell viability. Our results showed that the presence of biosilica from the GB, SN, AI, and PV sponges is non-cytotoxic. The only biosilica with limited cell compatibility (i.e., the GA-derived biosilica) demonstrates a higher concentration

of CaP structures on their surface after immersion in SBF. A possible explanation for the observed toxicity is the increment of pH generated from the release of cations from the biosilica structure, as has been observed for Bioglass (Brückner et al., 2016). In fact, we observed an increase in the pH of the medium after 3 days of incubation in the presence of biosilica particles, showing the highest value for GA-based biosilica (**Supplementary Table 1**). This result is consistent with the higher susceptibility of the cells to the extracts obtained from this type of biosilica, especially at higher concentrations, i.e., 100 and 50 mg/mL. In fact, this type of observation has been also reported by Wanandi et al. (2017) showing that the release of cations leads to the alkalinization of the culture medium, which, in turn, causes

cell death. Importantly, when reducing the concentration of the biosilica to 10 mg/mL, the cell viability is not affected. Moreover, the concentration of cations in the medium after 3 days of incubation (**Supplementary Table 2**), shows a significant reduction of P and Ca content in the medium (due to the deposition of CaP) while significantly increasing the Si content (a known promoter of osteogenesis) (Götz et al., 2019). These differences in the composition of the medium is consistent with the higher bioactivity of GA-derived biosilica and its ability to promote new bone formation. Overall, our results indicate that the GA-derived biosilica are suitable to be further tested in the context of BTE and regeneration.

CONCLUSION

In this study, biosilicas were obtained by calcination of five North Atlantic deep-sea sponges, i.e., *Geodia atlantica* (GA), *Geodia barretti* (GB), *Stelletta normani* (SN), *Axinella infundibuliformis* (AI), and *Phakellia ventilabrum* (PV), and their bioactivity was evaluated by incubation in SBF. Our results showed that the GB-based biosilica has a reduced capacity to promote the deposition of stable CaP structures. In addition, the SN-, AI-, and PV-based biosilicas demonstrated the capacity to generate some CaP domains in their surface, however, they are not stable over longer periods of time (i.e., 28 days). Overall, the biosilica obtained from GA presented the highest bioactivity, and it is not cytotoxic at a concentration of 10 mg/mL. Based on our findings we conclude that the GA-based biosilica (at a concentration up to 10 mg/mL) has potential to be used in BTE applications.

DATA AVAILABILITY STATEMENT

The original contributions presented in the study are included in the article/**Supplementary Material**, further inquiries can be directed to the corresponding author/s.

AUTHOR CONTRIBUTIONS

OD: research design, experimental work, data aquisition and treatment, discussion, and manuscript draft preparation. SA: experimental work, data aquisition and treatment, discussion, and contribution to manuscript writing. JRX: collecting, identification and characterization of the sponge species used in the work, and contribution to the discussion of the results. HTR: collecting, identification and characterization of the sponge species used in the work, and contribution to the discussion of the results. THS: research conceptualization and design, supervision, discussion, manuscript revision, funding acquisition, and project management. RAP: research conceptualization and design, supervision, discussion, manuscript writing and revision, funding acquisition, and project management. RLR: supervision, manuscript revision, funding acquisition, and project management.

FUNDING

SUPPLEMENTARY MATERIAL

The Supplementary Material for this article can be found online at: https://www.frontiersin.org/articles/10.3389/fmars.2021.637810/full#supplementary-material

REFERENCES

Amorim, S., Martins, A., Neves, N. M., Reis, R. L., and Pires, R. A. (2014). Hyaluronic acid/poly-l-lysine bilayered silica nanoparticles enhance the osteogenic differentiation of human mesenchymal stem cells. *J. Mater. Chem. B* 2, 6939–6946. doi: 10.1039/c4tb01071j

Antoniac, I., Lesci, I. G., Blajan, A. I., Vitioanu, G., and Antoniac, A. (2016). Bioceramics and biocomposites from marine sources. *Key Eng. Mater.* 672, 276–292.

Bailey, M. J., Coe, S., Grant, D. M., Grime, G. W., and Jeynes, C. (2009). Accurate determination of the Ca: P ratio in rough hydroxyapatite samples by SEM-EDS, PIXE and RBS – a comparative study. *X Ray Spectr.* 38, 343–347. doi: 10.1002/xrs.1171

Barros, A. A., Aroso, I. M., Silva, T. H., Mano, J. F., Duarte, A. R. C., and Reis, R. L. (2014). Surface modification of silica-based marine sponge bioceramics induce hydroxyapatite formation. *Cryst. Growth Des.* 14, 4545–4552. doi: 10.1021/cg500654u

Barros, A. A., Aroso, I. M., Silva, T. H., Mano, J. F., Duarte, A. R. C., and Reis, R. L. (2016). In vitro bioactivity studies of ceramic structures isolated from marine sponges. *Biomed. Mater.* 11:045004. doi: 10.1088/1748-6041/11/4/045004

Blunt, J. W., Copp, B. R., Munro, M. H. G., Northcote, P. T., and Prinsep, M. R. (2005). Marine natural products. *Nat. Prod. Rep.* 22, 15–61. doi: 10.1039/b415080p

Blunt, J. W., Copp, B. R., Munro, M. H. G., Northcote, P. T., and Prinsep, M. R. (2010). Marine natural products. *Nat. Prod. Rep.* 27, 165–237. doi: 10.1039/b906091j

Brückner, R., Tylkowski, M., Hupa, L., and Brauer, D. S. (2016). Controlling the ion release from mixed alkali bioactive glasses by varying modifier ionic radii and molar volume. *J. Mater. Chem. B* 4, 3121–3134. doi: 10.1039/C5TB02426A

Cárdenas, P., Rapp, H. T., Klitgaard, A. B., Best, M., Thollesson, M., and Tendal, O. S. (2013). Taxonomy, biogeography and DNA barcodes of Geodia species (Porifera, Demospongiae, Tetractinellida) in the Atlantic boreo-arctic region. *Zool. J. Linnean Soc.* 169, 251–311. doi: 10.1111/ZOJ.12056

Cha, J. N., Shimizu, K., Zhou, Y., Christiansen, S. C., Chmelka, B. F., Stucky, G. D., et al. (1999). Silicatein filaments and subunits from a marine sponge direct the polymerization of silica and silicones in vitro. *Proc. Natl. Acad. Sci.U.S.A.* 96, 361–365. doi: 10.1073/pnas.96.2.361

Diogo, G. S., Marques, C. F., Sotelo, C. G., Pérez-Marin, R. I., Pirraco, R. P., Reis, R. L., et al. (2020). Cell-laden biomimetially mineralized shark-skin-collagen-based 3d printed hydrogels for the engineering of hard tissues. *ACS Biomater. Sci. Eng.* 6, 3664–3672. doi: 10.1021/acsbiomaterials.0c00436

Diogo, G. S., Senra, E. L., Pirraco, R. P., Canadas, R. F., Fernandes, E. M., Serra, J., et al. (2018). Marine collagen/apatite composite scaffolds envisaging hard tissue applications. *Mar. Drugs.* 16:269. doi: 10.3390/md16080269

Dudik, O., Leonor, I., Xavier, J. R., Rapp, H. T., Pires, R. A., Silva, T. H., et al. (2018). Sponge-derived silica for tissue regeneration. *Mater. Today* 21, 577–578. doi: 10.1016/j.mattod.2018.03.025

Ehrlich, H., Demadis, K. D., Pokrovsky, O. S., and Koutsoukos, P. G. (2010a). Modern views on desilicification: biosilica and abiotic silica dissolution in natural and artificial environments. *Chem. Rev.* 110, 4656–4689. doi: 10.1021/cr900334y

Ehrlich, H., Deutzmann, R., Brunner, E., Cappellini, E., Koon, H., Solazzo, C., et al. (2010b). Mineralization of the metre-long biosilica structures of glass sponges is templated on hydroxylated collagen. *Nat Chem.* 2, 1084–1088. doi: 10.1038/nchem.899

Elango, J., Zhang, J., Bao, B., Palaniyandi, K., Wang, S., Wu, W., et al. (2016). Rheological, biocompatibility and osteogenesis assessment of fish collagen scaffold for bone tissue engineering. *Int. J. Biol. Macromol.* 91, 51–59. doi: 10.1016/j.ijbiomac.2016.05.067

Fernandes, J. S., Martins, M., Neves, N. M., Fernandes, M. H. V., Reis, R. L., and Pires, R. A. (2016). Intrinsic antibacterial borosilicate glasses for bone tissue engineering applications. *ACS Biomater. Sci. Eng.* 2, 1143–1150. doi: 10.1021/acsbiomaterials.6b00162

Fu, Q., Saiz, E., Rahaman, M. N., and Tomsia, A. P. (2011). Bioactive glass scaffolds for bone tissue engineering: state of the art and future perspectives. *Mater. Sci. Eng. C Mater. Biol. Appl.* 31, 1245–1256. doi: 10.1016/j.msec.2011.04.022

Gabbai-Armelin, P. R., Kido, H. W., Cruz, M. A., Prado, J. P. S., Ivanzi, I. R., Custódio, M. R., et al. (2019). Characterization and cytotoxicity evaluation of a marine sponge biosilica. *Mar. Biotechnol.* 21, 65–75. doi: 10.1007/s10126-018-9858-9

Götz, W., Tobiasch, E., Witzleben, S., and Schulze, M. (2019). Effects of silicon compounds on biomineralization, osteogenesis, and hard tissue formation. *Pharmaceutics* 11:117. doi: 10.3390/pharmaceutics11030117

Greasley, S. L., Page, S. J., Chen, S., Martin, R. A., Riveiro, A., Hanna, J. V., et al. (2016). Controlling particle size in the Stöber process and incorporation of calcium. *J. Colloid Interface Sci.* 469, 213–223. doi: 10.1016/j.jcis.2016.01.065

ISO 10993-5 (2009). *Biological Evaluation of Medical Devices – Part 5: Tests for in Vitro Cytotoxicity.* Available online at: http://nhiso.com/wp-content/uploads/2018/05/ISO-10993-5-2009.pdf

Jones, J. R., Sepulveda, P., and Hench, L. L. (2001). Dose-dependent behavior of bioactive glass dissolution. *J. Biomed. Mater. Res.* 58, 720–726. doi: 10.1002/jbm.10053

Kaur, G., Pandey, O. P., Singh, K., Homa, D., Scott, B., and Pickrell, G. (2014). A review of bioactive glasses: their structure, properties, fabrication and apatite formation. *J. Biomed. Mater. Res. A* 102, 254–274. doi: 10.1002/jbm.a.34690

Khan, A. S., Khalid, H., Sarfraz, Z., Khan, M., Iqbal, J., Muhammad, N., et al. (2017). Vibrational spectroscopy of selective dental restorative materials. *Appl. Spectrosc. Rev.* 52, 507–540. doi: 10.1080/05704928.2016.1244069

Kokubo, T., and Takadama, H. (2006). How useful is SBF in predicting in vivo bone bioactivity? *Biomaterials* 27, 2907–2915. doi: 10.1016/j.biomaterials.2006.01.017

Kulaev, I. S., Vagabov, V. M., and Kulakovskaya, T. V. (2005). *The Biochemistry of Inorganic Polyphosphates*, 2nd Edn. New York,NY: John Wiley & Sons.

Kulakovskaya, T. V., Vagabov, V. M., and Kulaev, I. S. (2012). Inorganic polyphosphate in industry, agriculture and medicine: modern state and outlook. *Process Biochem.* 74, 1–10. doi: 10.1016/j.procbio.2011.10.028

Le, T. D. H., Liaudanskaya, V., Bonani, W., Migliaresi, C., and Motta, A. (2018). Enhancing bioactive properties of silk fibroin with diatom particles for bone tissue engineering applications. *J. Tissue Eng. Regen. Med.* 12, 89–97. doi: 10.1002/term.2373

Lewandowska-Łańcucka, J., Fiejdasz, S., Rodzik, Ł., Koziel, M., and Nowakowska, M. (2015). Bioactive hydrogel-nanosilica hybrid materials: a potential injectable scaffold for bone tissue engineering. *Biomed. Mater.* 10:015020. doi: 10.1088/1748-6041/10/1/015020

Marris, E. (2006). Marine natural products: drugs from the deep. *Nature* 443, 904–905. doi: 10.1038/443904a

Müller, W. E. G., Schröder, H. C., Wiens, M., Perovi æ-Ottstadt, S., Batel, R., and Müller, I. M. (2004). Traditional and modern biomedical prospecting: part II-the benefits: approaches for a sustainable exploitation of biodiversity (secondary metabolites and biomaterials from sponges). *Evid. Based. Complement. Alternat. Med.* 1, 133–144. doi: 10.1093/ecam/neh030

Müller, W. E. G., Wang, X., Kropf, K., Boreiko, A., Schlossmacher, U., Brandt, D., et al. (2008). Silicatein expression in the hexactinellid *Crateromorpha meyeri*: the lead marker gene restricted to siliceous sponges. *Cell Tissue Res.* 333, 339–351. doi: 10.1007/s00441-008-0624-6

Odatsu, T., Azimaie, T., Velten, M. F., Vu, M., Lyles, M. B., Kim, H. K., et al. (2015). Human periosteum cell osteogenic differentiation enhanced by ionic silicon release from porous amorphous silica fibrous scaffolds. *J. Biomed. Mater. Res. Part A.* 103, 2797–2806. doi: 10.1002/jbm.a.35412

Rahaman, M. N., Day, D. E., Bal, B. S., Fu, Q., Jung, S. B., Bonewald, L. F., et al. (2011). Bioactive glass in tissue engineering. *Acta Biomater.* 7, 2355–2373. doi: 10.1016/j.actbio.2011.03.016

Rezwan, K., Chen, Q. Z., Blaker, J. J., and Boccaccini, A. R. (2006). Biodegradable and bioactive porous polymer/inorganic composite scaffolds for bone tissue engineering. *Biomaterials* 27, 3413–3431. doi: 10.1016/j.biomaterials.2006.01.039

Schröder, H. C., Boreiko, O., Krasko, A., Reiber, A., Schwertner, H., and Müller, W. E. G. (2005). Mineralization of SaOS-2 cells on enzymatically (silicatein) modified bioactive osteoblast-stimulating surfaces. *J. Biomed. Mater. Res. Part B Appl. Biomater.* 75, 387–392. doi: 10.1002/jbm.b.30322

Schröder, H. C., Wang, X., Tremel, W., Ushijima, H., and Müller, W. E. G. (2008). Biofabrication of biosilica-glass by living organisms. *Nat. Prod. Rep.* 25, 455–474. doi: 10.1039/b612515h

Silva, T. H., Alves, A., Ferreira, B. M., Oliveira, J. M., Reys, L. L., Ferreira, R. J. F., et al. (2012). Materials of marine origin: a review on polymers and ceramics of biomedical interest. *Int. Mater. Rev.* 57, 276–306. doi: 10.1179/1743280412Y.0000000002

Thakur, N. L., and Müller, W. E. G. (2004). Biotechnological potential of marine sponges. *Curr. Sci.* 86, 1506–1512.

Venkatesan, J., Anil, S., Chalisserry, E. P., and Kim, S. K. (2016). "Marine sponges as future biomedical models," in *Marine Sponges: Chemicobiological and Biomedical Applications*, eds P. Ramjee and E. Hermann (New Delhi: Springer India), 349–357. doi: 10.1007/978-81-322-2794-6_18

Wanandi, S. I., Yustisia, I., Neolaka, G. M. G., and Jusman, S. W. A. (2017). Impact of extracellular alkalinization on the survival of CD24-/CD44+human breast cancer stem cells associated with cellular metabolic shifts. *Braz. J. Med. Biol. Res.* 50, e6538. doi: 10.1590/1414-431X201176538

Wang, X., Schröder, H. C., Feng, Q., Draenert, F., and Müller, W. E. G. (2013). The deep-sea natural products, biogenic polyphosphate (bio-polyp) and biogenic silica (bio-silica), as biomimetic scaffolds for bone tissue engineering: fabrication of a morphogenetically-active polymer. *Mar. Drugs* 11, 718–746. doi: 10.3390/md11030718

Wang, X., Schröder, H. C., and Müller, W. E. G. (2018). Amorphous polyphosphate, a smart bioinspired nano-/bio-material for bone and cartilage regeneration: towards a new paradigm in tissue engineering. *J. Mater. Chem. B* 6, 2385–2412. doi: 10.1039/C8TB00241J

Wang, X., Schröder, H. C., Wiens, M., Ushijima, H., and Müller, W. E. G. (2012). Bio-silica and bio-polyphosphate: applications in biomedicine (bone

formation). *Curr. Opin. Biotechnol.* 23, 570–578. doi: 10.1016/j.copbio.2012.01.018

Wiens, M., Wang, X., Schloßmacher, U., Lieberwirth, I., Glasser, G., Ushijima, H., et al. (2010a). Osteogenic potential of biosilica on human osteoblast-like (SaOS-2) cells. *Calcif. Tissue Int.* 87, 513–524. doi: 10.1007/s00223-010-9408-6

Wiens, M., Wang, X., Schröder, H. C., Kolb, U., Schlossmacher, U., Ushijima, H., et al. (2010b). The role of biosilica in the osteoprotegerin/RANKL ratio in human osteoblast-like cells. *Biomaterials* 31, 7716–7725. doi: 10.1016/j.biomaterials.2010.07.002

Wysokowski, M., Jesionowski, T., and Ehrlich, H. (2018). Biosilica as a source for inspiration in biological materials science. *Am. Mineral.* 103, 665–691. doi: 10.2138/am-2018-6429

Xue, S.-H., Xie, H., Ping, H., Li, Q.-C., Su, B.-L., and Fu, Z.-Y. (2015). Induced transformation of amorphous silica to cristobalite on bacterial surfaces. *RSC Adv.* 5, 71844–71848. doi: 10.1039/c5ra13619a

Yu, B., Turdean-Ionescu, C. A., Martin, R. A., Newport, R. J., Hanna, J. V., Smith, M. E., et al. (2012). Effect of calcium source on structure and properties of sol-gel derived bioactive glasses. *Langmuir* 28, 17465–17476. doi: 10.1021/la303768b